Physics in Medicine & Biology



# Quantitative characterization of breast tissues with dedicated CT imaging

To cite this article before publication: Anna Piai *et al* 2019 *Phys. Med. Biol.* in press https://doi.org/10.1088/1361-6560/ab2c29

# Quantitative characterization of breast tissues with dedicated CT imaging

**Anna Piai**

Department of Physics, University of Trieste, Via Valerio 2, 34127 Trieste, Italy and INFN Division of Trieste, Via Valerio 2, 34127 Trieste, Italy ‡

**Adriano Contillo**

Department of Physics and Earth Sciences, University of Ferrara, Via Saragat 1, 44122 Ferrara, Italy and INFN Division of Ferrara, Via Saragat 1, 44122 Ferrara, Italy and Elettra-Sincrotrone Trieste S.C.p.A, 34149 Basovizza Trieste, Italy

E-mail: adriano.contillo@elettra.eu

**Fulvia Arfelli**

Department of Physics, University of Trieste, Via Valerio 2, 34127 Trieste, Italy and INFN Division of Trieste, Via Valerio 2, 34127 Trieste, Italy

**Deborah Bonazza**

Department of Medical Science, Cattinara Hospital, University of Trieste, Strada di Fiume 447, 34149 Trieste, Italy

**Luca Brombal**

Department of Physics, University of Trieste, Via Valerio 2, 34127 Trieste, Italy and INFN Division of Trieste, Via Valerio 2, 34127 Trieste, Italy

**Maria Assunta Cova**

Department of Medical Science, Cattinara Hospital, University of Trieste, Strada di Fiume 447, 34149 Trieste, Italy

**Pasquale Delogu**

Department of Physical sciences, Earth and Environment, University of Siena, Strada Laterina 8, 53100 Siena, Italy and INFN Division of Pisa, Largo Bruno Pontecorvo 3, 56127 Pisa, Italy

**Vittorio Di Trapani**

Department of Physical sciences, Earth and Environment, University of Siena, Strada Laterina 8, 53100 Siena, Italy and INFN Division of Pisa, Largo Bruno Pontecorvo 3, 56127 Pisa, Italy

‡ Present address: Department of Physics, University of Milan, Via G. Celoria 16, 20133 Milano, Italy

**Sandro Donato**

Department of Physics, University of Trieste, Via Valerio 2, 34127 Trieste, Italy and INFN Division of Trieste, Via Valerio 2, 34127 Trieste, Italy

**Bruno Golosio**

Department of Physics, University of Cagliari, Monserrato-Sestu, 09042 Monserrato, Italy and INFN Division of Cagliari, Monserrato-Sestu, 09042 Monserrato, Italy

**Giovanni Mettivier**

Department of Physics, University of Napoli Federico II, Via Cinthia, 80126 Fuorigrotta, Napoli, Italy and INFN Division of Napoli, Via Cinthia, 80126 Fuorigrotta, Napoli, Italy

**Piernicola Oliva**

Department of Chemistry and Pharmacy, University of Sassari, Via Vienna, 07100 Sassari SS, Italy and INFN Division of Cagliari, Monserrato-Sestu, 09042 Monserrato, Italy

**Luigi Rigon**

Department of Physics, University of Trieste, Via Valerio 2, 34127 Trieste, Italy and INFN Division of Trieste, Via Valerio 2, 34127 Trieste, Italy

**Angelo Taibi**

Department of Physics and Earth Sciences, University of Ferrara, Via Saragat 1, 44122 Ferrara, Italy and INFN Division of Ferrara, Via Saragat 1, 44122 Ferrara, Italy

**Maura Tonutti**

Department of Medical Science, Cattinara Hospital, University of Trieste, Strada di Fiume 447, 34149 Trieste, Italy

**Giuliana Tromba**

Elettra-Sincrotrone Trieste S.C.p.A, 34149 Basovizza Trieste, Italy

**Fabrizio Zanconati**

Department of Medical Science, Cattinara Hospital, University of Trieste, Strada di Fiume 447, 34149 Trieste, Italy

**Renata Longo**

Department of Physics, University of Trieste, Via Valerio 2, 34127 Trieste, Italy and INFN Division of Trieste, Via Valerio 2, 34127 Trieste, Italy

**Abstract.**

A quantitative characterization of the soft tissues composing the human breast is achieved by means of a monochromatic CT phase-contrast imaging system, through accurate measurements of their attenuation coefficients within the energy range of interest for breast CT clinical examinations. Quantitative measurements of linear attenuation coefficients are performed on tomographic reconstructions of surgical samples, using monochromatic X-ray beams from a synchrotron source and a free space propagation setup. An online calibration is performed on the obtained reconstructions, in order to reassess the validity of the standard calibration procedure of the CT scanner. Three types of healthy tissues (adipose, glandular, and skin) and malignant tumors, when present, are considered from each sample. The measured attenuation coefficients are in very good agreement with the outcomes of similar studies available in the literature, although they span an energy range that was mostly neglected in the previous studies. No globally significant differences are observed between healthy and malignant dense tissues, although the number of considered samples does not appear sufficient to address the issue of a quantitative differentiation of tumors. The study assesses the viability of the proposed methodology for the measurement of linear attenuation coefficients, and provides a denser sampling of attenuation data in the energy range useful to breast CT.

*Keywords*: breast CT, synchrotron radiation, phase-contrast imaging, linear attenuation coefficient

Submitted to: *Phys. Med. Biol.*

## 1. Introduction

Breast cancer is one of the most frequently diagnosed cancers and one of the leading causes of death for women worldwide. Early detection is therefore a key factor in treating and defeating this disease. However, the high contrast and spatial resolutions required make breast imaging one of the most challenging imaging modalities. Digital mammography, which is nowadays the primary screening and diagnostic modality, has still several limitations, mostly due to the superposition of tissues, that can hide or mask signs of malignancies, especially in dense breasts (Kolb 2002). For this reason, researchers carried out a significant effort during the last decades in investigating 3D imaging modalities. Among them, tomosynthesis is often used in clinical practice as a second-level examination (Sechopoulos 2013a, Sechopoulos 2013b). Breast Computed Tomography (BCT) instead, although not widely used clinically, is arising an increasing interest and several research groups worldwide performed clinical trials (Lindfors 2008, O'Connell 2010, Sarno 2016, Kalender 2017, Berger 2019). A few clinical systems are available commercially: the Friedrich-Alexander University of Erlangen-Nürnberg

(Germany)§ and the Rochester Medical Center (USA)‖ promoted startup companies to manufacture and commercialize their prototypes.

The SYRMA-3D (SYnchrotron Radiation for MAmmography) collaboration aims to perform the first *in vivo* breast computed tomography with synchrotron radiation (SR) using phase-contrast techniques at the SYRMEP (SYnchrotron Radiation for MEdical Physics) beamline of the Elettra synchrotron facility in Trieste (Longo 2016, Longo 2019). The use of SR can significantly improve the quality of Computed Tomography (CT) images. The high X-ray intensity on a broad energy range provides the possibility to obtain tunable monochromatic beams, avoiding beam hardening and allowing to optimize the dose delivered to the patient. Also a patient-based energy optimization, according to the large inter-individual variability of patients, can be obtained. Furthermore the high spatial coherence, produced by the combination of the small size of the source and the large source-to-sample distance, allows the implementation of the free space propagation phase-contrast imaging technique (Paganin 2002). As a result, an additional source of (phase) contrast, namely edge enhancement, adds to the absorption contrast which characterizes conventional imaging (Rigon 2014). Edge enhancement is due to the interference, which takes place during the free space propagation, between the unperturbed beam and the X-rays refracted at the interfaces within or at the edge of the sample. Although edge enhancement may add to the diagnostic value in planar imaging (Castelli 2011, Longo 2014), in CT studies an additional processing step, namely phase retrieval (PhR), is generally performed. The application of a PhR algorithm removes the edge enhancement and produces a gray level map which is proportional to the absorption image, and yet shows a significant improvement in signal to noise ratio (Gureyev 2017, Kitchen 2017, Brombal 2018a, Brombal 2018b). A formal introduction to this topic is given in Sec. 2.1.

The radiographic appearance of the breast is characterized by adjoining low contrast structures that encode the diagnostic information. Therefore, the accurate knowledge of the attenuation properties of breast tissues is essential to optimize the contrast between the different structures, thus obtaining a better image quality. Moreover, the better knowledge of the attenuation properties of samples provides an improvement in the calculation of the absorbed dose, yielding positive contributions to dosimetric models. In the field of breast X-ray diagnostic imaging the measurement of the linear attenuation coefficients of breast tissues is therefore of fundamental importance. However, despite their importance, such measurements are not widespread because of their implementation difficulties. Hammerstein and co-workers evaluated the linear attenuation coefficients of skin, fat and glandular breast tissues for the first time in the energy range of 10 to 50 keV, by determining the chemical composition of normal breast tissues (Hammerstein 1979). A recent study by Berggren and collaborators (Berggren

§ AB-CT – Advanced Breast-CT GmbH, Erlangen, Germany. https://www.ab-ct.com/. Accessed february 7, 2019.

‖ New York Koning Corporation, West Henrietta, NY. Koning breast CT. http://koninghealth.com/en/kbct. Accessed february 7, 2019.

2018) reports an effective atomic number of skin that confirms the results found by Hammerstein. Later, Johns and Yaffe measured the linear attenuation coefficients of breast tissues using a high-purity germanium spectroscopy system and X-rays beams in the energy range between 18 and 110 keV (Johns 1987). Fredenberg *et al.* measured the linear attenuation coefficients of solid (benign and malignant) breast lesions in the energy range from 15 to 40 keV using a spectral mammography system (Fredenberg 2016). They also measured the coefficients of malignant and normal (both glandular and adipose) tissues in the same energy range (Fredenberg 2018). Carroll and colleagues (Carroll 1994) and Tomal *et al.* (Tomal 2010) used instead monochromatic X-rays produced by a synchrotron source, avoiding in this way spectrometric techniques, and evaluated the linear attenuation coefficients of adipose and glandular breast tissues by direct attenuation measurements of thin samples selected as homogeneous as possible. Generally speaking, the energy sampling of these measurements was rather coarse, typically with steps of 5 to 10 keV.

SR BCT images allow measurements of linear attenuation coefficients from breast tissue samples with no need for any specific preparation. Chen and co-workers already used monochromatic and high-intensity SR BCT to evaluate the linear attenuation coefficients of surgical breast tissues in the energy range from 15 to 26.5 keV (Chen 2010).

All the previously described measurements provide an extremely coarse sampling of data in the energy range of interest for CT clinical exams (concerning BCT typically from 25 keV to 40 keV). In this work, we acquired SR BCT data of surgical breast samples in the energy range between 26 and 38 keV using monochromatic and high-flux SR in combination with a direct conversion CdTe photon counting detector. Reconstructed SR BCT images have been calibrated in order to obtain quantitative linear attenuation coefficient maps; the linear attenuation coefficients of skin, adipose, glandular, and tumor tissues from mastectomy and lumpectomy samples have been studied. For the first time to our knowledge, quantitative measurements have been performed on phase-retrieved images, which is allowed by the result of Gureyev and collaborators (Gureyev 2017) concerning the relationship between attenuation and phase-retrieved images. This study aims to validate the imaging chain of SYRMA-3D as a measuring device of breast tissues attenuation coefficients from an operational point of view, following the assessment of reconstruction accuracy and noise that was already carried out in a propaedeutical phantom study (Contillo 2018). The present validation includes a comparison of the obtained results to the ones previously published in literature.

Moreover, the possibility of discerning normal and tumor tissues has been investigated. In the framework of breast imaging, tissue differentiation is still an open issue. Johns and Yaffe, for example, showed that significant differences exist between adipose tissue and all other tissues at all energies, and that the glandular tissue and the infiltrating ductal carcinoma are only separated below 31 keV, overlapping significantly at higher energies (Johns 1987). Carroll and co-workers concluded instead that there is some degree of overlap between glandular and carcinoma tissues also at

these low energies (Carroll 1994). Tomal *et al.* found significant differences in the linear attenuation coefficient between glandular and malignant tissues at energies below 28 keV (Tomal 2010). No significant differences were found by Fredenberg *et al.* between benign and malignant lesions on the whole investigated energy range (Fredenberg 2016). Chen *et al.* were not able to distinguish between glandular tissue and malignant lesions (Chen 2010). The present study aims to provide additional evidence regarding the subject.

## 2. Methods

This section provides a description of the theoretical background and of the experimental setup employed in the analysis.

### *2.1. Theoretical background*

The high spatial coherence of the synchrotron source allows the implementation of a particular PhR modality based on free space propagation, often referred to as the Paganin method (Paganin 2002). At its core, such technique is the result of a two-step procedure: an *optical* forward convolution (the free space propagation) followed by a *numerical* backward deconvolution (the phase retrieval procedure). The procedure is schematically depicted in Fig. 1.

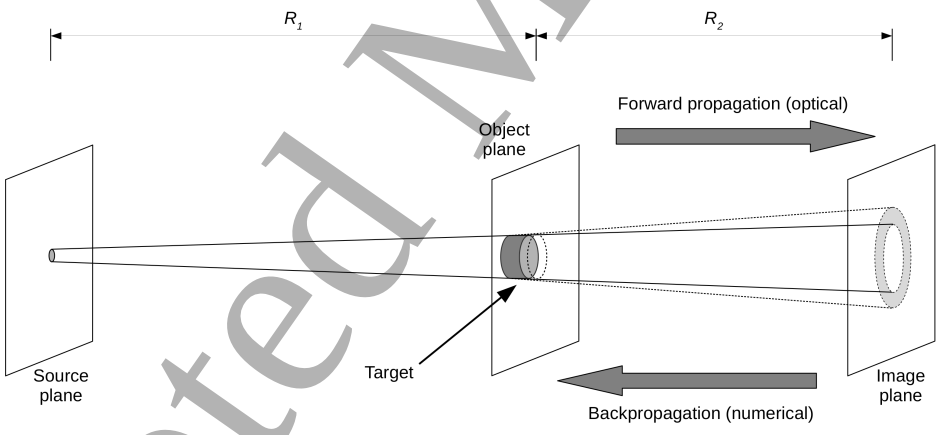


**Figure 1.** Schematic representation of the Paganin PhR method. The source-to-object distance and the object-to-image distance are labelled $R_1$ and $R_2$, respectively.

The kernel describing the free space propagation, according to the "Homogeneous Transfer of Intensity Equation (TIE-hom)" (Teague 1983, Paganin 2002), reads

$$1 - \sigma^2 \nabla^2 = 1 - \frac{\lambda R_2 \delta}{4\pi\beta} \nabla^2 \tag{1}$$

$\sigma^2$ encoding the transverse spread of the phase contrast effect ($\lambda$ being the beam wavelength, $R_2$ the object-to-image distance, $\delta$ and $\beta$ the components of the refraction

index of the target) and $\nabla^2$ being the Laplacian over the transverse dimensions. Obviously, the employment of the exact inverse kernel in the retrieval procedure leads to a retrieved image whose information content coincides with the one of a non-propagated image, at most up to a multiplicative constant related to the normalization of the retrieval kernel. In other words, the technique consists in a subsequent "addition + subtraction" of the phase-contrast effect, resulting in a pure attenuation image – to the extent of the coincidence between the refraction index components employed in the retrieval kernel and the ones pertaining to the actual imaged sample. In the present implementation, the refraction index components were chosen as the ones pertaining to the "breast tissue" listed in a database provided by the University of Melbourne¶.

Despite the apparent circularity, it was pointed out by Gureyev *et al.* (Gureyev 2017) that the Paganin method leads to a strong decrease in the noise variance of retrieved images without affecting their spatial resolution. Such result was explained by noticing that the free propagation leaves the noise variance of the image essentially unchanged, while the retrieval procedure reduces it drastically, as expected by any numerical convolution. On the other hand, the effects of the two steps on the spatial resolution are basically inverse to each other, leading to an overall conservation of the resolution. As explained by Gureyev, the origin of such "unreasonable" enhancement lies in the fact that an optical convolution (as opposed to a numerical one) is applied prior to the image detection, *before* the generation of detection noise, which is therefore not propagated by the convolution. Preliminary experimental validations of this theoretical prediction were recently provided by Kitchen and colleagues (Kitchen 2017) and by Brombal and collaborators (Brombal 2018b).

The above considerations imply that the Paganin method provides a "cleaner" version of a hypothetical non-propagated image, thus preserving the contrasts of intensity between adjacent structures of the imaged target. Therefore, it allows an equivalent quantitative measurement of the attenuation coefficients of imaged tissues. As a consequence of such equivalence, the calibration procedure of the SYRMA-3D imaging setup (which was originally introduced as applied to pure attenuation images in Contillo 2018) can be straightforwardly extended to the PhR-based measurements performed in the present analysis. The details of the calibration will be discussed in Sec. 2.2 and 3.

### *2.2. Experimental setup*

The acquisitions were performed at the SYRMEP beamline, at the Elettra synchrotron facility in Trieste, Italy, using photons produced in the ring operating at 2.4 GeV. The X-ray beam is produced by one of the storage ring bending magnets of the synchrotron machine. A Si(111) double-crystal monochromator, working in Bragg configuration, allows to obtain a monochromatic beam in the energy range 8.5-40 keV, selecting the energy with a resolution of $\Delta E/E \sim 10^{-3}$. The beam cross section in the patient room

¶ http://ts-imaging.science.unimelb.edu.au/Services/Simple/ICUtilXdata.aspx

is 220 mm (horizontal) × 3.5 mm (vertical, Gaussian shape, FWHM) with a small divergence (7 mrad (horizontal) × 0.2 mrad (vertical)) (Tromba 2010). The samples were imaged hanging from the patient support, a rotating table with an ergonomically designed aperture at the rotation center, designed to perform both mammography and BCT. Thanks to the small divergence of the beam within the object (*i.e.* parallel-beam geometry), the projections were collected over 180°. Given the small beam vertical dimension, in order to scan the whole breast, the patient support allows movements in the vertical direction. The beam leaving the object impinges on the detector, placed about 1.6 m from the patient position. The object-to-detector distance, along with the laminar shape of the beam, allows working in a scatter-free geometry without the need of anti-scattering grids (Longo 2016, Longo 2019).

Radiation doses were evaluated by means of an automatic script encoding the results of an *ad hoc* Monte Carlo simulation, based on a GEANT4 code optimized for breast dosimetry, which, given the measured air kerma and entering the sample dimension and glandularity, returns the mean glandular dose $MGD_t$ (Fedon 2015, Mettivier 2016). Samples were scanned with one or two distinct nominal doses, namely 5 mGy and 20 mGy, which correspond to reference dose values of SYRMA-3D for diagnostic (*in vivo*) acquisition and "high image quality" (*ex vivo*) acquisition modalities, respectively. The latter value is the dose considered as reference standard (that is, as upper limit) during the first cone-beam BCT clinical trials (O'Connell 2012).

Data are collected with PIXIRAD-8, a large-area high efficiency direct-conversion CdTe photon counting device (Bellazzini 2013, Delogu 2016). PIXIRAD-8 is made up of eight modules, pixels are hexagonal in shape and are arranged on a honeycomb matrix with a horizontal pitch of 60 $\mu$m and a vertical pitch of 52 $\mu$m. Therefore, for a slice thickness of about 52 $\mu$m, projections of 3.5 mm height result in 66 reconstructed slices.

Images produced by the detector undergo an *ad hoc* pre-processing procedure, developed by the SYRMA-3D collaboration (Brombal 2018c). It has a modular structure comprising four steps: a dynamic flat fielding (Delogu 2017), to correct pixel-to-pixel non uniformity and polarization time dependent gain variations; a seaming, to close the dead space between adjacent blocks; the removal of speckles due to bad pixels and a dynamic ring removal, to remove ring artifacts produced by gain inhomogeneities at the pixel level. A PhR filter is applied to pre-processed data and finally images are reconstructed via a filtered back-projection with a standard Shepp-Logan filtering.

The analyzed surgical samples were fixed in formalin, sealed in a vacuum bag and conserved at 4°C. Their maximum diameters ranged from 8 cm (sample 6, see Fig. 2) to 17 cm (sample 4). All the procedures adopted in this work followed the Directive 2004/23/EC of the European Parliament and of the Council of 31 March 2004 on setting standards of quality and safety for the donation, procurement, testing, processing, preservation, storage, and distribution of human tissues. The images reported in this study were acquired to guide the pathologist in the localization of lesions for the histological examination, according to the standard procedures of the Pathology Unit of the Academic Hospital of Cattinara, Trieste University. The samples were derived

**Table 1.** Acquisition parameters of the analyzed samples. The entries *yes* and *no* indicate the presence or absence of the tissue in each sample, respectively. In the sixth column, the entries *ductal* and *lobular* imply the presence of a tumor and indicate the typology of infiltrating carcinoma.

| sample | energies (keV) | online cal | adipose | gland | tumor | skin |
|---|---|---|---|---|---|---|
| 1 | 28,32,35,38 | yes | yes | no | ductal | yes |
| 2 | 28,32,35,38 | yes | yes | yes | lobular | no |
| 3 | 28,32,35 | yes | yes | no | ductal | no |
| 4 | 26,28,30,32,34,36,38 | yes | yes | yes | no | no |
| 5 | 28,32 | no | yes | no | ductal | yes |
| 6 | 32,35,38 | no | yes | yes | ductal | yes |
| 7 | 28,38 | no | yes | no | no | yes |

from surgical material sent to the Pathology Unit of the University Hospital of Trieste (Italy) according to local guidelines for histological examination.

In conventional tomography, where polychromatic beams are used, each voxel in the reconstructed slice is assigned a number, referred to as the CT number and measured in Hounsfield Units. Such unit of measure is intrinsically defined as relative to the attenuation coefficient of water. Conversely, when a monochromatic radiation is used, as in the framework of the SYRMA-3D study, the filtered back-projection algorithm allows to reconstruct a map of gray levels that is directly proportional to the attenuation coefficients of the imaged object (see also Brombal 2019). In order to retrieve the linear attenuation coefficients (in $cm^{-1}$), SR BCT images need a calibration procedure. An offline calibration procedure is already available for the imaging device, making use of a dedicated test object (Contillo 2018) containing water and a set of plastic inserts (polyethylene, nylon, polyoxymethylene and polytetrafluoroethylene) mimicking the attenuation properties of soft tissues. In order to make an online check of the effectiveness of the calibration, an *ad hoc* procedure was applied to some of the surgical specimens. For this purpose, four samples are provided with three test vials, placed in the periphery of the field of view and filled with reference materials of known linear attenuation coefficients (ethanol, water, and glycerol). For each one of the reference materials, the theoretical linear attenuation coefficient is calculated, for each given energy, from the XMuDat X-ray database (Nowotny 1998), while the measured value is computed as the average, over the 66 slices, of the mean values of specified regions of interest (ROIs), placed in a homogeneous region of the reference material. The associated error coincides with the sample standard deviation. Seven surgical samples are analyzed in this study: they are shown in Fig. 2 and a brief description of the nature of the lesions is reported in the caption of the figure. The acquisition parameters are given in Tab. 1 and Tab. 2. Of course, the various tissues of each sample were only included in the analysis when it was possible to select an acceptably broad uniform region of said tissue.

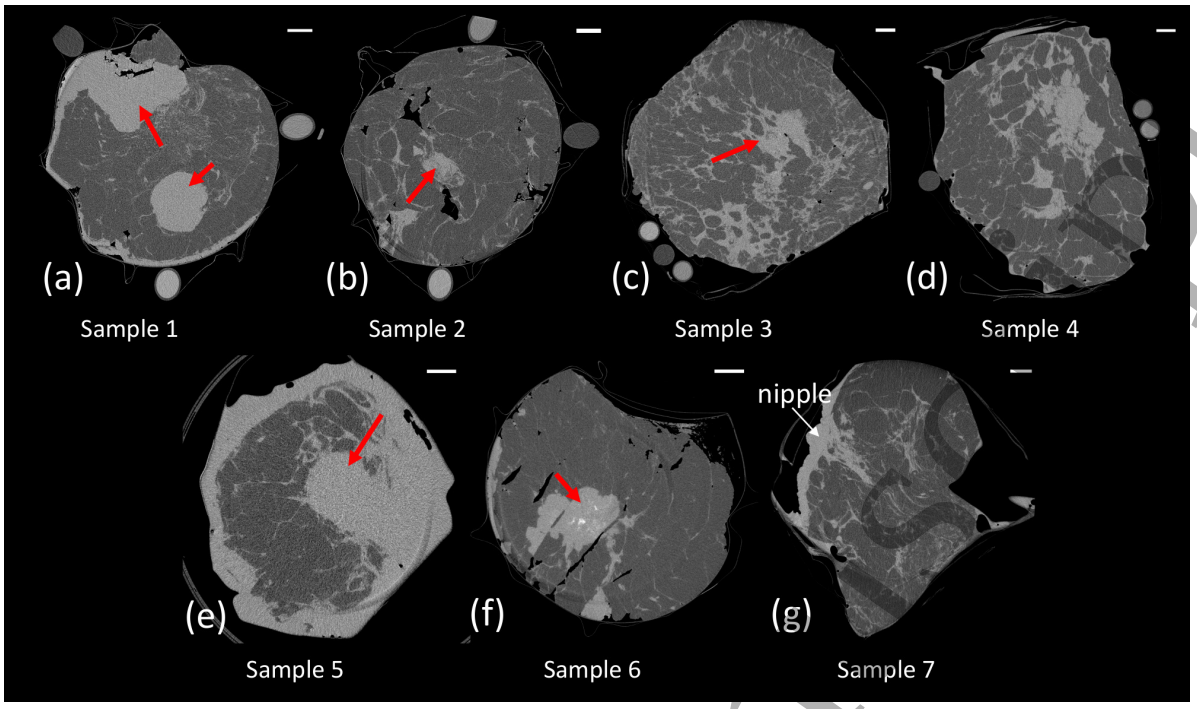


**Figure 2.** Analyzed surgical samples. When present, the red arrows show the position of the lesion. The white bars on the top right corner of each image represent 1 cm lengths. (a) sample 1: vastly differentiated infiltrating ductal carcinoma; (b) sample 2: infiltrating lobular carcinoma; (c) sample 3: infiltrating ductal carcinoma; (d) sample 4: risk reducing mastectomy (no lesion); (e) sample 5: infiltrating ductal carcinoma; (f) sample 6: infiltrating ductal carcinoma with a core of desmoplastic tissue; (g) sample 7: infiltrating ductal carcinoma, located outside of the volume portion imaged in the present study.

## 3. Results

Fig. 3 depicts the measured voxel values derived from the SR BCT images versus the theoretical linear attenuation coefficients, obtained from the online calibration of sample 1 (acquired at 32 keV with a 5 mGy dose) and from the offline calibration (also at 32 keV with a 5 mGy dose). The straight lines correspond to the linear fits.

The two calibration procedures are compared to evaluate the reproducibility of the system. For this purpose the linear attenuation coefficients of the reference materials (*i.e.* ethanol, water, and glycerol) are measured applying both offline and online calibration equations; given the fit parameters $p_0$ and $p_1$ and the mean gray level $\bar{x}$, the calibrated values are computed as

$$\mu(cm^{-1}) = p_1 \cdot \bar{x}(a.u.) + p_0. \tag{2}$$

Examples of fit parameters for both the online and the offline calibration are reported in Tab. 3.

In order to evaluate the relative accuracy of the two calibrations we measured, for each acquisition energy and each reference material, the relative difference between the

**Table 2.** Radiation doses to the analyzed samples, with references to the corresponding nominal doses (5 mGy and/or 20 mGy).

| sample | energies (keV) | nominal (mGy) | $MGD_t$ (mGy) | air Kerma (mGy) |
|---|---|---|---|---|
| 1 | 28 | 5 | 5.2 | 8.4 |
| | 32 | 5/20 | 5.2/21.0 | 7.0/28.5 |
| | 35 | 5 | 5.1 | 6.2 |
| | 38 | 5 | 5.1 | 5.9 |
| 2 | 28 | 5/20 | 5.2/20.1 | 8.4/32.6 |
| | 32 | 5/20 | 5.3/20.6 | 7.2/27.9 |
| | 35 | 5/20 | 5.1/20.1 | 6.2/24.8 |
| | 38 | 5/20 | 5.1/20.4 | 5.9/23.4 |
| 3 | 28 | 5/20 | 5.1/20.9 | 10.2/42.0 |
| | 32 | 5/20 | 5.1/19.4 | 8.0/30.8 |
| | 35 | 5/20 | 5.0/20.2 | 7.0/28.2 |
| 4 | 26 | 20 | 20.3 | 47.6 |
| | 28 | 20 | 20.1 | 40.4 |
| | 30 | 20 | 20.6 | 36.4 |
| | 32 | 20 | 20.6 | 32.6 |
| | 34 | 20 | 20.5 | 29.7 |
| | 36 | 20 | 20.6 | 27.8 |
| | 38 | 20 | 20.3 | 25.8 |
| 5 | 28 | 5 | 5.2 | 10.4 |
| | 32 | 5 | 5.1 | 8.0 |
| 6 | 32 | 5/20 | 5.2/20.3 | 7.0/27.5 |
| | 35 | 5 | 5.2 | 6.4 |
| | 38 | 5 | 5.0 | 5.8 |
| 7 | 28 | 5/20 | 5.2/19.9 | 8.4/32.3 |
| | 38 | 5/20 | 5.0/20.2 | 5.7/23.3 |

**Table 3.** Examples of fit parameters obtained from the calibration of phase-retrieved images as a function of the energy: the offline calibration is performed following the procedure of Contillo 2018, while the online calibration refers to the one performed on sample 1.

| energy (keV) | offline | | online | |
|---|---|---|---|---|
| | $p_0 \pm \sigma_{p_0}$ ($cm^{-1}$) | $p_1 \pm \sigma_{p_1}$ ($cm^{-1}$) | $p_0 \pm \sigma_{p_0}$ ($cm^{-1}$) | $p_1 \pm \sigma_{p_1}$ ($cm^{-1}$) |
| 28 | 0.008 ± 0.004 | 186.4 ± 0.4 | -0.0002 ± 0.0010 | 180.4 ± 1.1 |
| 32 | -0.0001 ± 0.0012 | 185.2 ± 0.6 | 0.009 ± 0.003 | 180.8 ± 1.6 |
| 35 | 0.004 ± 0.002 | 184.9 ± 0.6 | 0.0016 ± 0.0011 | 179.6 ± 0.8 |
| 38 | 0.002 ± 0.002 | 185.5 ± 0.5 | -0.0014 ± 0.0010 | 179.7 ± 1.0 |

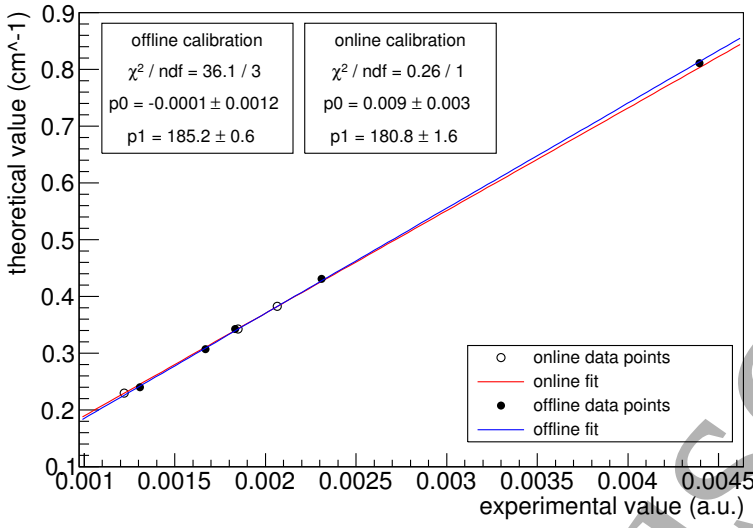


**Figure 3.** Example of linear fits obtained from the online calibration of sample 1 (acquired at 32 keV with a 5 mGy dose) and from the offline calibration at 32 keV (following the procedure proposed in Contillo 2018). The standard deviations of the measured values are of the order of 0.1% and thus, due to their small size, error bars are not distinguishable from the markers. The fit parameters $p_0$, $p_1$, and the $\chi^2$ are reported for each calibration procedure.

predicted attenuation coefficients:

$$\text{diff}_{\%} = 100 \cdot \frac{|\mu_{online} - \mu_{offline}|}{\mu_{offline}}. \tag{3}$$

The mean $\text{diff}_{\%}$ parameter, computed by averaging the results obtained from different samples acquired at different energies is $\text{diff}_{\%} = 1.0\%$ ($\text{diff}_{\%,max} = 3.5\%, \sigma = 0.7\%$). Such a good result allows to rely on the offline calibration, that is more suitable to be included in the routine quality control procedures of the imaging device. Therefore, the remainder of the analysis will be devoted to the sole offline calibration.

The absolute accuracy of the offline calibration is also evaluated by comparing the measured linear attenuation coefficients with the theoretical ones (obtained from XMuDat database), following the definition adopted in Contillo 2018:

$$\text{accuracy} = 100 \cdot \frac{|\mu_{th} - \mu_{meas}|}{\mu_{th}}. \tag{4}$$

The following average value is obtained: accuracy = 0.72% (max = 2.69%, $\sigma = 0.65$ %).

As a side analysis, the offline calibration given above (obtained in phase retrieval mode) was compared to the one given in Contillo 2018 (obtained in pure absorption mode), using a measure of relative difference equivalent to the one of Eq. 3. Such parameter represents a genuine, phantom-based comparison between the phase-retrieved images and pure absorption images. It was found $\text{diff}_{\%} = 1.1\%$ ($\text{diff}_{\%,max} = 2.4\%, \sigma =$

0.7%), which guarantees a very good level of agreement between the two reconstruction methods.

The offline calibration equations are then applied to calculate the linear attenuation coefficients of breast tissues following Eq. 2. The corresponding gray level values are measured on circular ROIs, of varying sizes selected to be contained in homogeneous regions of the tissues, and averaged over the 66 reconstructed slices. The corresponding errors are calculated with the propagation of uncertainty. Since the tissue morphology changed in the vertical direction, the position of the ROIs had to be varied by hand, slice by slice, to ensure the ROIs were always contained in a homogeneous region of tissue.

Tab. 4 reports the mean linear attenuation coefficients for the four types of breast tissue (adipose and glandular tissues, skin, and tumor) at different energies. Since not all tissues are embedded in each specimen, which was not acquired at every available energy, the number of samples used to evaluate the mean value of each tissue is also reported in the table.

The linear attenuation coefficients of adipose, glandular tissues, and tumor are compared with the ones previously published in literature: depicted in Fig. 4 are our measured linear attenuation coefficients of adipose, glandular, and tumor tissues versus the X-ray energy in the range from 15 keV to 50 keV. The data points were obtained as combined means and standard deviations of the various samples considered in the study. For comparison, data from the aforementioned sources are presented as well. Although no direct measurements are available in the literature regarding the skin, Hammerstein *et al.* reported a measure of its chemical composition. Therefore, an explicit comparison with our results (also shown in Fig. 4) was obtained by recovering the linear attenuation coefficient of the skin from its composition making use of the XMuDat database. For the sake of completeness, an equivalent recovery was also performed from the skin composition provided by the ICRU Report 46 (White 1992), also represented in Fig. 4. It can be seen that the overlap between the two recovered attenuations is not complete, meaning that the original chemical compositions are slightly different.

All the literature data points are fitted against an effective function $f$ constructed as the sum of two power laws with respect to energy $E$

$$f(E) = \sum_{i=1}^{2} \alpha_i \, E^{-\beta_i} \,, \tag{5}$$

suitable to encode the transition between the photoelectric-dominated and the Compton-dominated regimes of the linear attenuation coefficients. These trend lines are reported in Fig. 4 alongside the corresponding confidence bands, calculated at 68% (that is, 1 standard deviation) for a straightforward comparison with the error bars of the data points.

Moreover, the linear attenuation coefficients of breast tissues measured from different samples are compared to evaluate inter-individual variability. The results

**Table 4.** Measured linear attenuation coefficients of breast tissues. $N$ refers to the number of investigated samples.

| Beam energy | | Linear attenuation coefficients ($cm^{-1}$) | | | |
|---|---|---|---|---|---|
| | | adipose | glandular | tumor | skin |
| 26 keV | N | 1 | 1 | 0 | 0 |
| | minimum | - | - | - | - |
| | mean | **0.321** | **0.496** | - | - |
| | maximum | - | - | - | - |
| 28 keV | N | 6 | 2 | 4 | 3 |
| | minimum | 0.281 | 0.423 | 0.420 | 0.423 |
| | mean | **0.287** | **0.428** | **0.430** | **0.424** |
| | maximum | 0.296 | 0.433 | 0.437 | 0.425 |
| 30 keV | N | 1 | 1 | 0 | 0 |
| | minimum | - | - | - | - |
| | mean | **0.273** | **0.395** | - | - |
| | maximum | - | - | - | - |
| 32 keV | N | 6 | 3 | 5 | 3 |
| | minimum | 0.249 | 0.352 | 0.351 | 0.352 |
| | mean | **0.254** | **0.355** | **0.362** | **0.360** |
| | maximum | 0.257 | 0.359 | 0.385 | 0.371 |
| 34 keV | N | 1 | 1 | 0 | 0 |
| | minimum | - | - | - | - |
| | mean | **0.245** | **0.338** | - | - |
| | maximum | - | - | - | - |
| 35 keV | N | 5 | 2 | 4 | 2 |
| | minimum | 0.233 | 0.319 | 0.316 | 0.321 |
| | mean | **0.236** | **0.321** | **0.325** | **0.326** |
| | maximum | 0.240 | 0.322 | 0.345 | 0.332 |
| 36 keV | N | 1 | 1 | 0 | 0 |
| | minimum | - | - | - | - |
| | mean | **0.233** | **0.312** | - | - |
| | maximum | - | - | - | - |
| 38 keV | N | 5 | 3 | 3 | 3 |
| | minimum | 0.221 | 0.292 | 0.294 | 0.296 |
| | mean | **0.224** | **0.295** | **0.302** | **0.300** |
| | maximum | 0.228 | 0.298 | 0.317 | 0.304 |

obtained from the analysis of samples acquired at 32 keV and 38 keV are depicted in Fig. 5.

Finally, the possibility of distinguishing normal dense tissues (gland and skin) from tumor is investigated. For this purpose the linear attenuation coefficients of breast tissues are compared at different energies. Fig. 6 shows the results obtained from the analysis of samples 1, 2, 5, and 6, the only samples containing both a normal dense tissue (gland and/or skin) and a tumor.

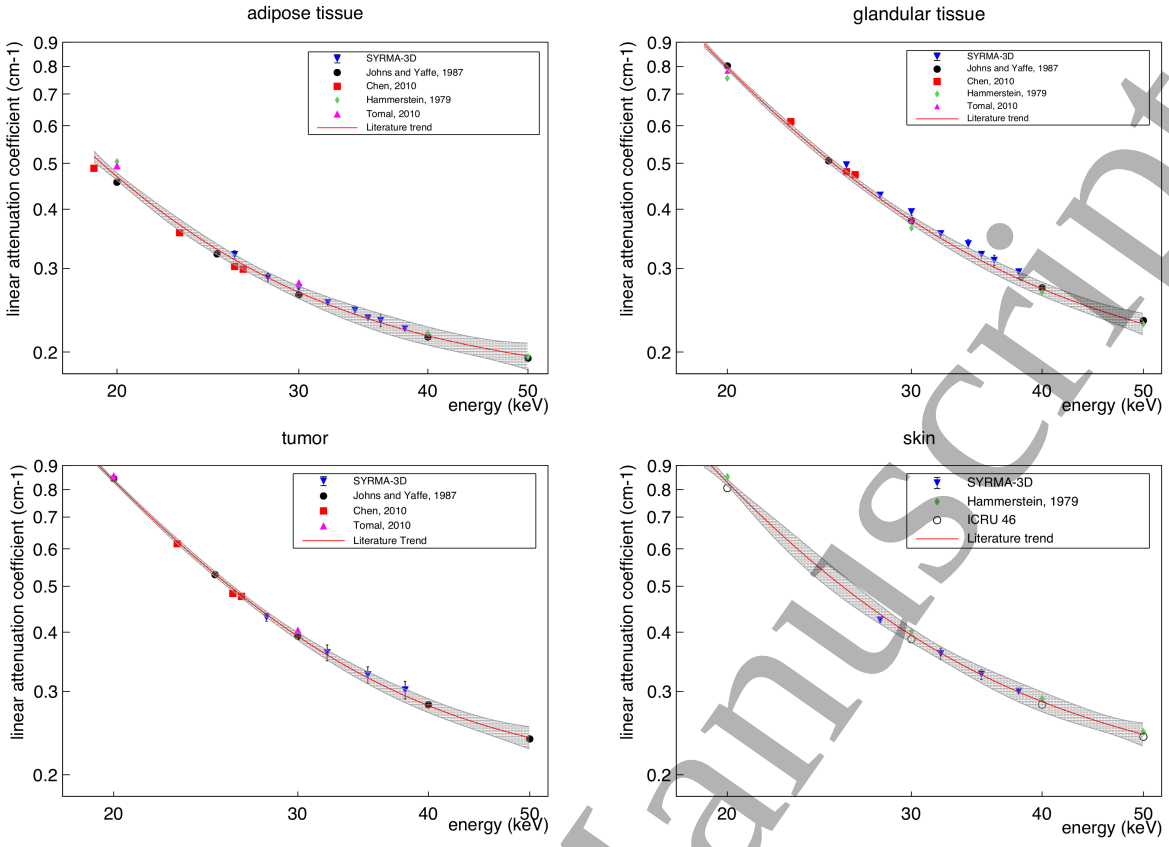


**Figure 4.** Comparison of the measured linear attenuation coefficients with the previously published data. Literature trend lines, and the corresponding 68% confidence bands, are reported in each plot. Due to their small size, the error bars of SYRMA-3D data points are often barely distinguishable from the markers, with the exception of tumors (a justification of this feature is given in Sec. 4 in terms of inter-individual variability of the measurements). Concerning the plot labelled "skin", the data from Hammerstein *et al.* and from ICRU 46 were extrapolated from their measurements of chemical composition.

## 4. Discussion

Offline calibration is a standardized procedure included in routine QC controls. The online check with the *ad hoc* calibration verifies the effectiveness of the procedure. Moreover, the obtained absolute accuracy is well within the 2.5% limit prescribed by the European guidelines on quality criteria for computed tomography (Menzel 2000). This result confirms the possibility to perform accurate quantitative measurements during the planned *in vivo* clinical session and encourages to lower the prescribed tolerance level for accuracy test.

The graphs in Fig. 4 show an excellent agreement with the data previously published in literature, as 95% of the SYRMA-3D data points are compatible within 1 standard deviation with the literature trends. In fact, the residual discrepancy is ascribable to a slight positive systematic of the glandular tissue, although the only actual source of incompatibility is the point at 26 keV (which is obtained from a single sample, as

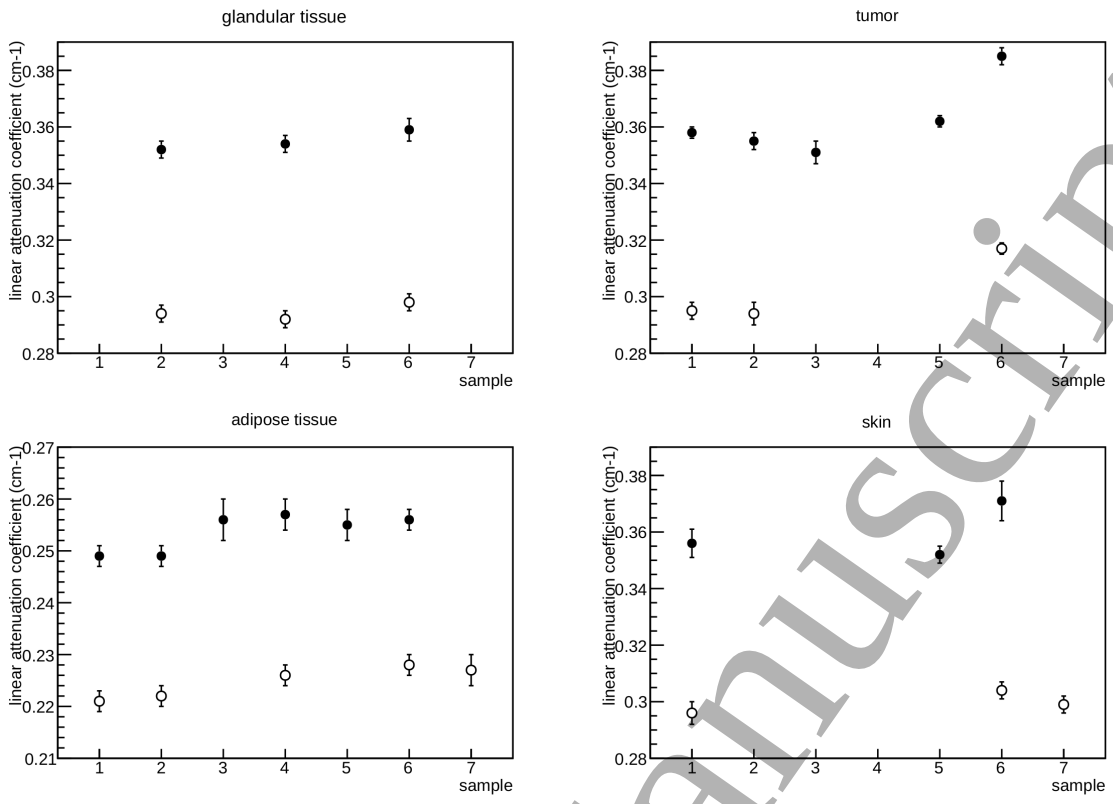


**Figure 5.** Linear attenuation coefficients of breast tissues measured from different samples at 32 keV (full markers) and 38 keV (open markers). Error bars represent 1 standard deviation. The vertical range of the plot referring to adipose tissue is different from the others because it is the only non dense tissue.

reported in Tab. 4). The other tissues are totally compatible. Additional findings are reported in the energy range of interest of breast CT clinical exams (between 26 keV and 38 keV), which received limited attention in the literature. Furthermore, innovative data are obtained regarding the skin (see Tab. 4). Based on our results the skin shows attenuation properties comparable with those of glandular tissue and tumor. It is probably worth noting that the results of Tab. 4 locate the skin tissue among the dense tissues, alongside gland and tumor. Such finding contrasts the assumption made by Dance and collaborators (Dance 1990) in the design of the breast model for dosimetric Monte Carlo simulations, where the skin was parameterized by a 5 mm layer of adipose tissue.

As far as the given measurements are concerned, none of the attenuation coefficients seems to carry a significant amount of inter-individual variability. No significant differences among different samples are observed regarding adipose tissue, glandular tissue and skin (values are compatible within 2 standard deviations). A similar conclusion holds for the tumor, with the exception of sample 6, whose attenuation coefficient is inconsistent with the ones obtained from the other samples both at 32 keV and 38 keV (see Fig. 5). The histological examination of sample 6 reveals the

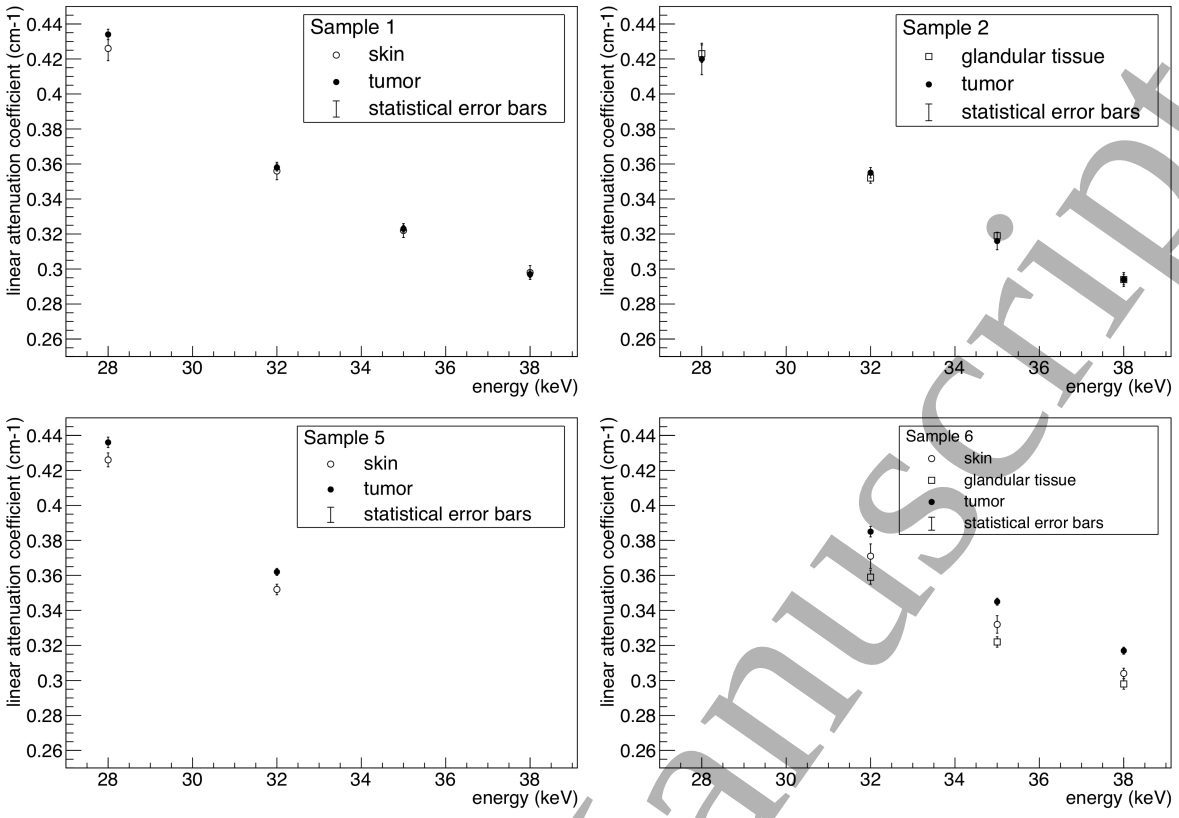


**Figure 6.** Linear attenuation coefficients of normal (skin and glandular) and tumor tissues at different energies measured from samples 1, 2, 5, and 6. Error bars represent 1 standard deviation.

presence of a ductal infiltrating cancer with a core of desmoplastic tissue (see Fig. 7). Therefore, the observed discrepancy is thought to be related to the nature of the lesion. Such findings show a partial disagreement with respect to some of the results of the previous literature: Tomal *et al.* find standard deviations among individuals of about 6-7%, while Johns and Yaffe find total variations of about 8%. However, it has to be noted that the number of samples considered in this study is probably too small to draw definitive conclusions: more accurate results will be available after the acquisition of a larger number of samples, both from surgical specimens and *in vivo* measurements during the upcoming clinical trial.

Concerning the use of formalin, it was found by Chen and collaborators (Chen 2010) that the fixation leads to a reduction of about 3% in the attenuation coefficient of glandular and tumor tissues, for energies around 20 keV. No significant effects were observed in the adipose tissue. A recent study by Fredenberg *et al.* (Fredenberg 2018) confirmed those findings, also reporting that the reduction on the dense tissues drops below 2% for energies $\gtrsim$30 keV, reaching 1% at 40 keV. Such differences are smaller than the fluctuations in the literature data shown in Fig. 4, which were obtained from fresh tissue (Hammerstein, Johns and Yaffe), from fixed tissue (Tomal), and from both fresh and fixed tissue (Chen).

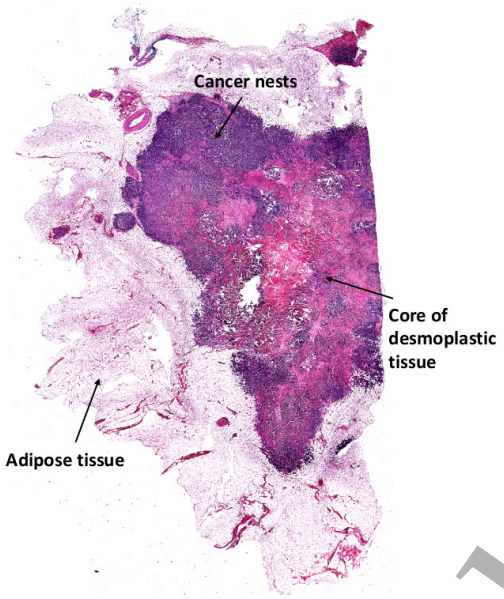


**Figure 7.** Histological image of sample 6. A core of desmoplastic tissue with numerous small cancer nests in the peripherical area of the lesion (darker region - ductal infiltrating cancer of the breast); the remaining white area is adipose tissue with vascular and lymphatic structures.

Finally, also the possibility of discerning tumor and normal tissues seems to depend on the nature of the lesion. For samples 1 and 2, which are characterized by an infiltrating ductal carcinoma and an infiltrating lobular carcinoma, respectively, the linear attenuation coefficients of tumor tissue and normal tissues (skin for sample 1 and glandular tissue for sample 2) overlap at all energies. Also for sample 5, which is characterized by an infiltrating carcinoma, the linear attenuation coefficients of skin and tumor are compatible within 2 standard deviations both at 28 keV and 32 keV. For sample 6, instead, the linear attenuation coefficient of tumor tissue is significantly higher than that of glandular tissue. Tumor and skin are instead compatible within 3 standard deviations. As in the case of inter-individual variability investigation, also in this case more accurate results will be provided when a larger number of samples will be available.

## 5. Conclusions

The accurate knowledge of the attenuation properties of breast tissues constitutes an important factor in the effectiveness of mammographic imaging techniques, for both the optimization of the image quality and the accurate estimate of the delivered radiation dose. The scientific literature on the subject includes measurements of the attenuation coefficients of the tissues composing the breast (adipose and glandular tissues, tumors), obtained by means of several radiological and spectrometric techniques.

The synchrotron-based breast imaging device developed by the SYRMA-3D

collaboration allows tomographic reconstructions that exhibit an extremely high resolution while accurately preserving the contrasts among the various structures of the imaged target. On the other hand, tomographic reconstructions performed with monochromatic spectra are known to provide explicit estimates of the attenuation coefficients pertaining to the reconstructed voxels. Therefore, the measurement of the attenuation coefficients of breast tissues represents a straightforward employment of the device.

Generally speaking, the results reported in the present analysis are in excellent agreement with the literature. In addition, for the first time to our knowledge, the attenuation coefficients of skin tissues of the breast were also investigated. The measurements presented here lie between 26 and 38 keV, an energy range coarsely sampled in the previous studies.

No significant differences were found between the attenuation coefficients of the dense tissues (gland, skin, and tumor), with the sole exception of a tumor exhibiting a vast core of desmoplastic tissue. However, it is worth noting that the number of specimens investigated here is probably insufficient to draw definite conclusions regarding the issue. We plan to extend the present analysis to the larger sample that will be provided by the forthcoming clinical trial.

## Acknowledgements

The authors gratefully acknowledge all the members of the project for their support on experimental and analysis activities. SYRMA-3D project is supported by Istituto Nazionale di Fisica Nucleare (National Scientific Committee 5 for Technological and interdisciplinary research) and Elettra-Sincrotrone Trieste SCpA and collaborates with the Cattinara University Hospital. Sandro Donato is partially supported by Consorzio per la Fisica Trieste.

## References

Bellazzini R, Spandre G, Brez A, Minuti M, Pinchera M and Mozzo P 2013 Chromatic X-ray imaging with a fine pitch CdTe sensor coupled to a large area photon counting pixel ASIC *J. Instrum.* **8** C02028

Berger N, Marcon M, Saltybaeva N, Kalender WA, Alkadhi H, Frauenfelder T and Boss A 2019 Dedicated Breast Computed Tomography With a Photon-Counting Detector: Initial Results of Clinical In Vivo Imaging *Invest. Radiol.* accepted

Berggren K, Eriksson M, Hall P, Wallis M G and Fredenberg E 2018 In vivo measurement of the effective atomic number of breast skin using spectral mammography *Phys. Med. Biol.* **63** 215023

Brombal L *et al* 2018 Monochromatic breast computed tomography with synchrotron radiation: phase-contrast and phase-retrieved image comparison and full-volume reconstruction *J. Med. Imaging* **6** 031402

Brombal L *et al* 2018 Phase-contrast breast CT: the effect of propagation distance *Phys. Med. Biol.* **63** 24NT03

Brombal L, Donato S, Brun F, Delogu P, Fanti V, Oliva P, Rigon L, Di Trapani V, Longo R and Golosio B 2018 Large-area single-photon-counting CdTe detector for synchrotron radiation

computed tomography: a dedicated pre-processing procedure. *J. Synchrotron Radiat.* **25** 1068-1077

Brombal L, Kallon G, Jiang J, Savvidis S, De Coppi P, Urbani L, Forty EJ, Chambers R C, Olivo A and Endrizzi M 2019 Monochromatic propagation-based phase-contrast microscale computed-tomography system with a rotating-anode source *Phys. Rev. Applied.* **11** 034004

Carroll F E, Waters J W, Andrews W W, Price R R, Pickens D R, Willcott R, Tompkins P, Roos C, Page D and Reed G 1994 Attenuation of monochromatic X-rays by normal and abnormal breast tissues *Invest. Radiol.* **29** 266-272

Castelli E *et al* 2011 Mammography with Synchrotron Radiation: First Clinical Experience with Phase-Detection Technique *Radiology* **259** 3

Chen R C *et al* 2010 Measurement of the linear attenuation coefficients of breast tissues by synchrotron radiation computed tomography *Phys. Med. Biol.* **55** 4993

Contillo A, Veronese A, Brombal L, Donato S, Rigon L, Taibi A, Tromba G, Longo R and Arfelli F 2018 A proposal for a quality control protocol in breast CT with synchrotron radiation *Radiol. Oncol.* **52** 329-336

Dance D R 1990 Monte Carlo calculation of conversion factors for the estimation of mean glandular breast dose *Phys. Med. Biol.* **35** 1211-9

Delogu P, Oliva P, Bellazzini R, Brez A, De Ruvo P L, Minuti M, Pinchera M, Spandre G and Vincenzi A 2016 Characterization of Pixirad-1 photon counting detector for X-ray imaging *J. Instrum.* **11** P01015

Delogu P, Brombal L, Di Trapani V, Donato S, Bottigli U, Dreossi D, Golosio B, Oliva P, Rigon L and Longo R 2017 Optimization of the equalization procedure for a single-photon counting CdTe detector used for CT *J. Instrum.* **12** C11014

Fedon C, Longo F, Mettivier G and Longo R 2015 Geant4 for breast dosimetry: parameters optimization study *Phys. Med. Biol.* **60** N311

Fredenberg E, Kilburn-Toppin F, Willsher P, Moa E, Danielsson M, Dance D R, Young K C and Wallis M G 2016 Measurement of breast-tissue x-ray attenuation by spectral mammography: solid lesions *Phys. Med. Biol.* **61** 2595

Fredenberg E, Willsher P, Moa E, Dance D R, Young K C and Wallis M G 2018 Measurement of breast-tissue x-ray attenuation by spectral imaging: fresh and fixed normal and malignant tissue *Phys. Med. Biol.* **63** 235003-235003

Gureyev T E, Nesterets Y I, Kozlov A, Paganin D M and Quiney H M 2017 On the "unreasonable" effectiveness of transport of intensity imaging and optical deconvolution *JOSA A* **34** 2251-2260

Hammerstein G R, Miller D W, White D R, Ellen Masterson M, Woodard H Q and Laughlin J S 1979 Absorbed radiation dose in mammography *Radiology* **130** 485-91

Johns P C and Yaffe M J 1987 X-ray characterisation of normal and neoplastic breast tissues *Phys. Med. Biol.* **32** 675

Kalender W A, Kolditz D, Steiding C, Ruth V, Lück F, Rößler A-C and Wenkel E 2017 Technical feasibility proof for high-resolution low-dose photon-counting CT of the breast *Eur. Radiol.* **27** 1081-1086

Kitchen M J, Buckley G A, Gureyev T E, Wallace M J, Andres-Thio N, Uesugi K, Yagi N and Hooper SB 2017 CT dose reduction factors in the thousands using X-ray phase contrast *Sci. Rep.* **7** 15953

Kolb T M, Lichy J and Newhouse J H 2002 Comparison of the performance of screening mammography, physical examination, and breast US and evaluation of factors that influence them: An analysis of 27,825 patient evaluations *Radiology* **225** 165-175

Lindfors K K, Boone J M, Nelson T R, Yang K, Kwan A L C and Miller D F 2008 Dedicated breast CT: initial clinical experience *Radiology* **246** 725-733

Longo R *et al* 2014 Clinical study in phase-contrast mammography: image-quality analysis *Phil. Trans. R. Soc. A* **372** 20130025

Longo R *et al* 2016 Towards breast tomography with synchrotron radiation at Elettra: first images *Phys. Med. Biol.* **61** 1634

Longo R *et al* 2019 Advancements towards the implementation of clinical phase-contrast breast computed tomography at Elettra *J. Synchrotron Rad.* **26** accepted

Menzel H G S H *et al* 2000 European guidelines on quality criteria for computed tomography *Luxembourg: European Commission* **16262**

Mettivier G, Fedon C, Di Lillo F, Longo R, Sarno A, Tromba G and Russo P 2016 Glandular dose in breast computed tomography with synchrotron radiation *Phys. Med. Biol.* **61** 569-587

Nowotny R. XMuDat: Photon attenuation data on PC. *IAEA Report IAEA-NDS.* 1998; 195.

O'Connell A M, Conover D L, Zhang Y, Seifert P, Logan-Young W, Lin C-F L, Sahler L and Ning R 2010 Cone-beam CT for breast imaging: Radiation dose, breast coverage, and image quality *Am. J. Roentgenol.* **195** 496-509

O'Connell A M and Kawakyu-O'Connor D 2012 Dedicated cone-beam breast computed tomography and diagnostic mammography: comparison of radiation dose, patient comfort, and qualitative review of imaging findings in BI-RADS 4 and 5 lesions *J. Clin. Imaging Sci.* **2** 1-8

Paganin D, Mayo S C, Gureyev T E, Miller P R and Wilkins S W 2002 Simultaneous phase and amplitude extraction from a single defocused image of a homogeneous object *J. Microsc.* **206** 33-40

Rigon L 2014 x-Ray imaging with coherent sources *Comprehensive Biomedical Physics* **2** (Oxford: Elsevier)

Sarno A, Mettivier G, Di Lillo F, Cesarelli M, Bifulco P and Russo P 2016 Cone-beam micro computed tomography dedicated to the breast. *Med. Eng. Phys.* **38** 1449-1457

Sechopoulos I 2013 A review of breast thomosynthesis. Part I. The image acquisition process *Med. Phys.* **40** 014301-014301

Sechopoulos I 2013 A review of breast thomosynthesis. Part II. Image reconstruction, processing and analysis, and advanced applications *Med. Phys.* **40** 014302-014302

Teague M R 1983 Deterministic phase retrieval: a Greens function solution. *J. Opt. Soc. Am.* **73** 1434-1441

Tomal A, Mazarro I, Kakuno E M and Poletti M E 2010 Experimental determination of linear attenuation coefficient of normal, benign and malignant breast tissues. *Radiat. Meas.* **45** 1055-1059

Tromba G *et al* 2010 The syrmep beamline of elettra: clinical mammography and bio-medical applications *AIP Conference Proceedings* **1266** 18-23

White D R, Griffith R V and Wilson I J 1992 *Report 46* Journal of the International Commission on Radiation Units and Measurements